ACS NANOSCIENCE Au
AN OPEN ACCESS JOURNAL OF THE AMERICAN CHEMICAL SOCIETY

pubs.acs.org/nanoau

Article

Colloidal Synthesis and Photocatalytic Properties of Cu_3NbS_4 and Cu_3NbSe_4 Sulvanite Nanocrystals

Chen-Yu Chang, Roberto Prado-Rivera, Mimi Liu, Cheng-Yu Lai,* and Daniela R. Radu*

Cite This: *ACS Nanosci. Au* 2022, 2, 440–447

Read Online

ACCESS | Metrics & More | Article Recommendations | Supporting Information

ABSTRACT: Niobium sulvanites Cu_3NbX_4 (X = S, Se) have been theoretically predicted as promising candidates for solar photovoltaics and photocatalytic water splitting. This report outlines the first synthesis of Cu_3NbS_4 and Cu_3NbSe_4 in a nanocrystalline form. The crystal structures were investigated by X-ray diffraction, identity was confirmed by Raman spectroscopy, and the optoelectronic properties and morphology of Cu_3NbS_4 and Cu_3NbSe_4 nanocrystals were examined by UV–vis spectroscopy and transmission electron microscopy, respectively. To gain insight into the Cu_3NbX_4 formation, a mechanistic study was conducted for Cu_3NbSe_4 monitoring the nanoparticles' formation as a function of reaction time. Methylene blue photodegradation tests were conducted to evaluate the photoactivity of Cu_3NbS_4 and Cu_3NbSe_4. The degradation rates, 2.81×10^{-2} min^{-1} and 1.22×10^{-2} min^{-1} proved the photocatalysts' potential of nanoscale Cu_3NbX_4.

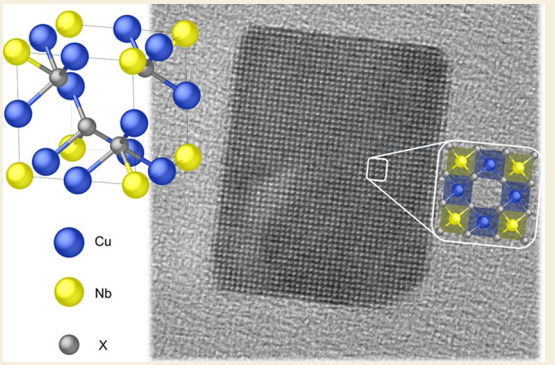

KEYWORDS: *nanocrystals, sulvanite, 2D transition-metal dichalcogenides (2D TMDCs), colloidal synthesis, solution-phase synthesis, catalysis*

The compounds in the class of sulvanite Cu_3MX_4 (M–group 5 metal: V, Nb, or Ta; X–chalcogen: S, Se, or Te) have received recent attention as potential photovoltaic (PV) absorbers, transparent conductors, ion conductors, and photocatalysts.[1−3] In addition, the parent compound, Cu_3VS_4, is a naturally occurring mineral, which names the series—"sulvanite"—and is composed of earth-abundant elements, resonant with the research community's interests in sustainable materials. The Cu_3VS_4 crystal structure was uncovered by Pauling in 1933;[4] the structure is comprised of CuX_4 and edge-sharing MX_4 tetrahedrons (Figure 1a).[5]

The significant progress in solution-processed chalcogenides for optoelectronic applications[6−9] drove the interest in synthesizing nanosulvanites. Nanocrystals and quasi-2D nanosheets of Cu_3VS_4 and Cu_3VSe_4 have been prepared using a solution-phase process.[10−12] The syntheses of nanoscale vanadium and tantalum crystalline sulvanites were also reported recently.[11−13] Based on reported UV–vis data, the vanadium sulvanites appear to possess an intermediate band, making them promising candidates for the absorber layer in solar PV.[2,11,12,14−17] However, nanoscale Cu_3NbS_4 and Cu_3NbSe_4 have not been reported to date; a few existing literature reports focus on the bulk niobium sulvanites, typically prepared by solid-state methods.[3,18] The optoelectronic properties of Cu_3MX_4 are dictated by their chemical composition, the compounds exhibiting a range of band gap values. Previous studies have shown the bulk Nb and Ta sulvanites to have optical band gaps of 2.5, 2.14, 2.54, and 2.32 eV for Cu_3NbS_4, Cu_3NbSe_4, Cu_3TaS_4, and Cu_3TaSe_4, respectively.[11,19−21]

Solid solutions of sulvanites with either V and Nb or V and Ta ($Cu_3Nb_{1-x}V_xS_4$ or $Cu_3Ta_{1-x}V_xS_4$) prepared by a solid-state method maintained the sulvanite structure and proved to be effective as hydrogen evolution cocatalysts with ruthenium (Ru) for photocatalytic water splitting under visible light.[20]

Chen et al. demonstrated that the optoelectronic properties of $Cu_3NbS_{4-x}Se_x$ prepared by conventional solid-state synthesis could be tuned using a mixed chalcogen approach.[20] The direct band gap of the prepared $Cu_3NbS_{4-x}Se_x$ (x = 0, 0.1, 0.2, 0.4, 0.6, 0.8, and 4) series was shown to decrease from 2.53 eV (x = 0.1) to 2.43 eV (x = 0.8) by increasing the Se substitution.[3]

In parallel with experimental work, theoretical predictions of the niobium sulvanites band gaps have also been published. Using first-principles calculations, Kehoe et al. predicted that Cu_3NbS_4 and Cu_3NbSe_4 possess optical band gaps of 2.31 and 1.95 eV, respectively.[2]

Received: April 25, 2022
Revised: June 11, 2022
Accepted: June 13, 2022
Published: June 24, 2022

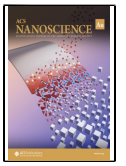

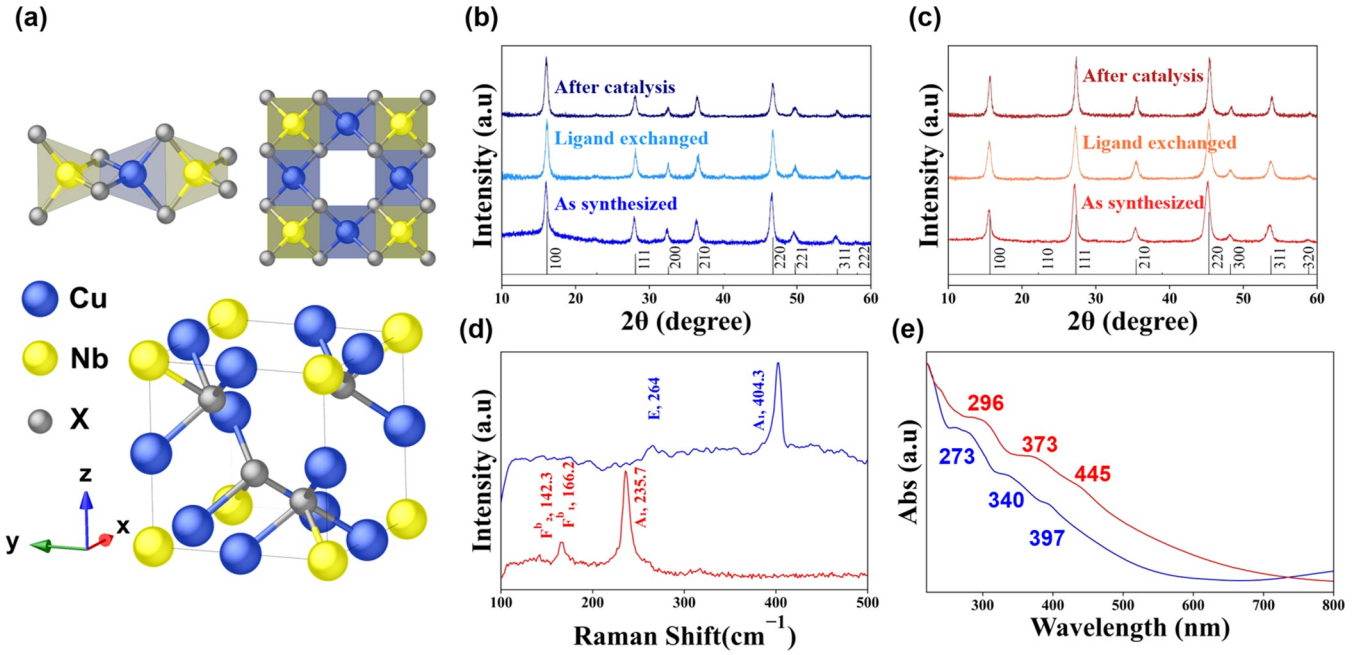

Figure 1. (a) Unit cell of Cu_3NbX_4 (X = S or Se) and structural details of atom arrangement; (b) X-ray diffraction of the Cu_3NbS_4 nanocrystals as-synthesized, post-ligand exchange, and post-catalysis (labeled blue lines); the line pattern is the reference from the PDF4 database (PDF Entry No. 04-004-0099); (c) X-ray diffraction of the Cu_3NbSe_4 nanocrystals as-synthesized, post-ligand exchange, and post-catalysis (labeled red lines); the line pattern is the reference (PDF Entry No. 04-001-6695); and (d) Raman scattering patterns of Cu_3NbS_4 (top, blue) and Cu_3NbSe_4 (bottom, red). Identified peaks match the literature. (e) UV−vis spectrum of Cu_3NbS_4 (blue) and Cu_3NbSe_4 (red).

Theoretical calculations also showed a large difference between the calculated electron (40 cm^2/v-s) and hole (164 cm^2/v-s) mobilities in sulvanites.[22] Due to their large band gap and significant charge carrier separation ability, Cu_3NbX_4 were predicted to be potential candidates for the hole transport layer in perovskite solar cells.[23] This charge carrier separation ability is expected to suppress recombination.

The ability to generate niobium sulvanites at the nanoscale could therefore expand their application palette by enabling their solution processing, popular for printed photovoltaics, large surface area catalysts, and flexible electronics. With respect to photocatalysis, the nanocrystal morphology renders a large surface area of the synthesized sulvanite nanocrystals, relative to bulk, potentially increasing the catalytic efficiency given the increased access to catalytic sites during photocatalytic reactions. In addition, visible-light photocatalytic activity is significant for environmental applications.[24]

We report, herein, facile colloidal synthesis of Cu_3NbX_4 (X = S, Se) nanoparticles. The advantages of colloidal synthesis include a low reaction temperature, shorter reaction time, and controlled particle size and morphology. X-ray powder diffraction (XRD) and Raman spectroscopy were used to validate the Cu_3NbX_4 (X = S, Se) nanoparticles' crystal structures. Transmission electron microscopy (TEM) confirmed the nanoscale morphology and crystallinity, and ultraviolet−visible (UV−vis) spectroscopy was used to determine the optical properties. Time-dependent studies were conducted to uncover the formation mechanism of Cu_3NbX_4 nanocrystals in the proposed approach, which uses the corresponding group 5 transition-metal dichalcogenide as an intermediate to form sulvanites by the addition of a copper salt. Methylene blue (MB) degradation experiments were used to observe the photocatalytic activity of Cu_3NbX_4 (X = S, Se). It is hypothesized that the charge carriers generated under illumination lead to the degradation of the MB.[25,26]

CHARACTERIZATION

The crystal structure of the Cu_3NbX_4 unit cell and the atomic arrangement, generated using CrystalMaker software, are shown in Figure 1a. The cell parameters of Cu_3NbS_4 and Cu_3NbSe_4 are 5.445 and 5.616 Å, respectively, as calculated by density functional theory (see the Supporting Information (SI) Computational Details).

XRD analysis of the synthesized Cu_3NbS_4 and Cu_3NbSe_4 (Figure 1b−c) confirmed that the sulvanite nanocrystals possess a cubic crystal structure belonging to the $P\bar{4}3m$ space group. The XRD pattern of Cu_3NbS_4 and Cu_3NbSe_4 nanocrystals shows pure Cu_3NbS_4 (PDF#04-004-0099) and Cu_3NbSe_4 (PDF#04-001-6695), respectively.

To prepare the nanocrystals for the catalysis experiments, a ligand exchange process was conducted to remove the long alkyl chain ligands that originated from the synthesis. The ligand exchange does not affect the nanocrystals' crystal structure. Furthermore, after the catalysis experiments, the nanocrystals preserve their structure, showing chemical stability. (Figure 1b−c).

Raman spectroscopy was used to confirm the identities of the synthesized Cu_3NbS_4 and Cu_3NbSe_4 nanocrystals (Figure 1d). The Raman spectra are in agreement with the computational work reported by Espinosa-García et al.[27] As shown in Figure 1d (top, blue line), the Cu_3NbS_4 Raman peaks at 264 and 404.3 cm^{-1} correspond to the E and A_1 vibration modes, matching well with the values of 269.62 and 403.87 cm^{-1}, as reported by Espinosa-García. For Cu_3NbSe_4, (Figure 1d, bottom, red line) the peaks at 235.7, 166.2, and 142.3 cm^{-1} correspond to A_1, F_1^b, and F_2^b, respectively, consistent with the

https://doi.org/10.1021/acsnanoscienceau.2c00021
ACS Nanosci. Au 2022, 2, 440−447

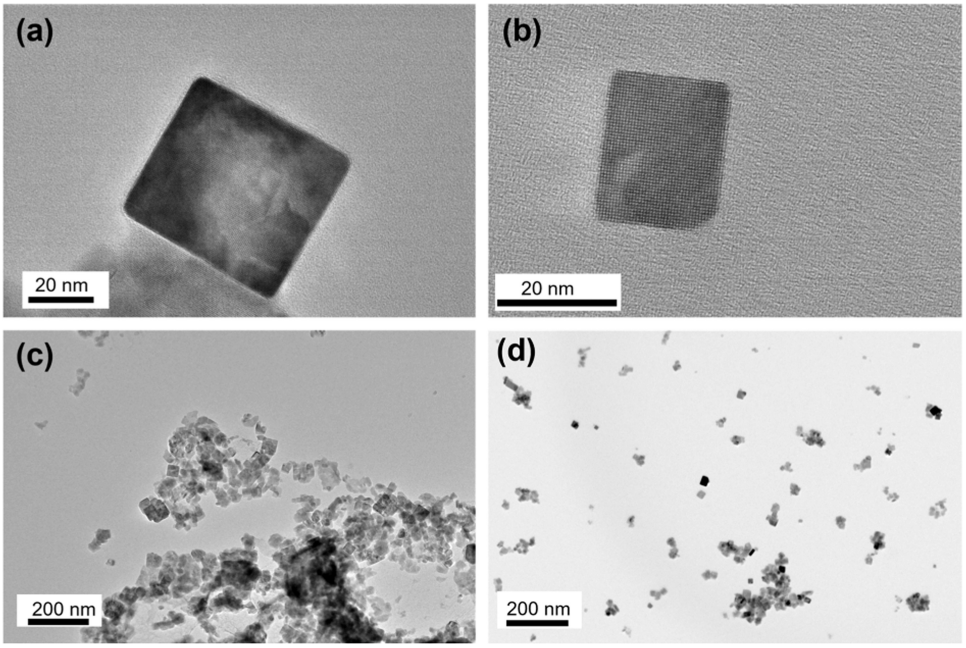

Figure 2. High-magnification TEM of (a) Cu_3NbS_4 and (b) Cu_3NbSe_4. Low-magnification TEM of (c) Cu_3NbS_4 and (d) Cu_3NbSe_4.

reported values of 236.44, 169.72, and 147.18 cm^{-1} (same report).[27]

Figure 1e shows the UV−visible spectra measured for both Cu_3NbS_4 and Cu_3NbSe_4. Three absorption peaks can be observed for both Cu_3NbS_4 (273, 340, and 397 nm) and Cu_3NbSe_4 (296, 373, and 445 nm). Similarly, density functional theory (DFT)-simulated absorption (Figure S2) also demonstrated three peaks; these can be attributed to direct optical transitions between the transition-metal d-states and chalcogen p-states largely at the Γ- and *X*-points of the valence and the conduction bands.[2]

The synthesized Cu_3NbS_4 and Cu_3NbSe_4 (Figure 2) exhibit cuboid morphology, illustrated in the TEM images. The average lengths for Cu_3NbS_4 are 39.00 ± 10.30 nm (long side) and 29.27 ± 10.06 nm (short side), while Cu_3NbSe_4 has an average length of 22.25 ± 6.7 nm (long side) and 15.33 ± 4.94 nm (short side). The particle size distribution can be found in Figure S3. Based on the cubic crystal structure of the sulvanite-type compounds, the height of the particles is estimated to be equivalent to or close to the other dimensions reported above.

Nanoparticle Formation Mechanism

Due to the similarity of Cu_3NbS_4 and Cu_3NbSe_4 in regard to their chemical composition, crystal structure, and synthesis procedure, the formation mechanism was exemplified herein for Cu_3NbSe_4, assuming that Cu_3NbS_4 will follow the same pattern.

To identify possible intermediates, at predetermined times, the Cu_3NbSe_4 synthesis reaction was quenched, and the resulting powder was analyzed by XRD. The quenching times were 5, 8, 15, 30, 60, and 120 min. The XRD-monitored time study reveals two remarkable changes, as follows (Figure 3). First, the characteristic XRD peaks for $Cu_{2-x}Se$ copper selenide appear right after the copper precursor injection (5 min). Second, 30 min after the Cu injection, the characteristic peaks of Cu_3NbSe_4, (100) at 16° and (200) at 36° appear in the pattern. A small shift of these characteristic diffraction peaks toward lower 2θ angle values could be seen when compared to the reference pattern. This slight and consistent shift across all

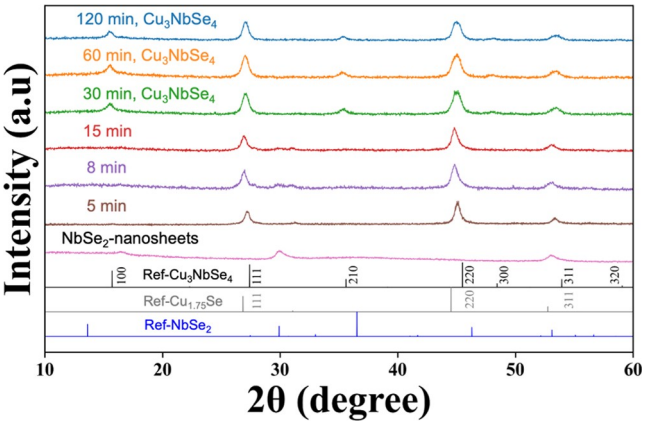

Figure 3. Time-dependent XRD mechanistic study of Cu_3NbSe_4 formation after the injection of the copper precursor.

characteristic peaks could be ascribed to size confinement and internal strain within the nanocrystal, both of which are reported in the literature to cause shifting and/or broadening of XRD peaks.[28−31] As the nanocrystal is formed, the *d*-spacing changes from its bulk values, thereby inducing strain. Further details are given in the Supporting Information (SI).

To further elucidate the nanocrystal formation mechanism, the reaction products were analyzed using a scanning transmission electron microscope equipped with energy-dispersive X-ray spectroscopy (STEM-EDX) (Figure 4). At 5 min after the Cu precursor addition, crystalline $Cu_{2-x}Se$ nanocrystals were identified in the image, as confirmed by XRD. This result indicates that $Cu_{2-x}Se$ is formed at the expense of the excess Se in the reaction as well as the Se resulting from the gradual decomposition of $NbSe_2$ nanosheets. The Nb redissolved in the reaction mixture and captured on the TEM appears in close proximity to $Cu_{2-x}Se$. At 30 min, the overlapping Nb and the $Cu_{2-x}Se$ suggest the progress of a Nb cation reaction with $Cu_{2-x}Se$ and the gradual formation of Cu_3NbSe_4. A Nb concentration gradient could be

https://doi.org/10.1021/acsnanoscienceau.2c00021
ACS Nanosci. Au 2022, 2, 440−447

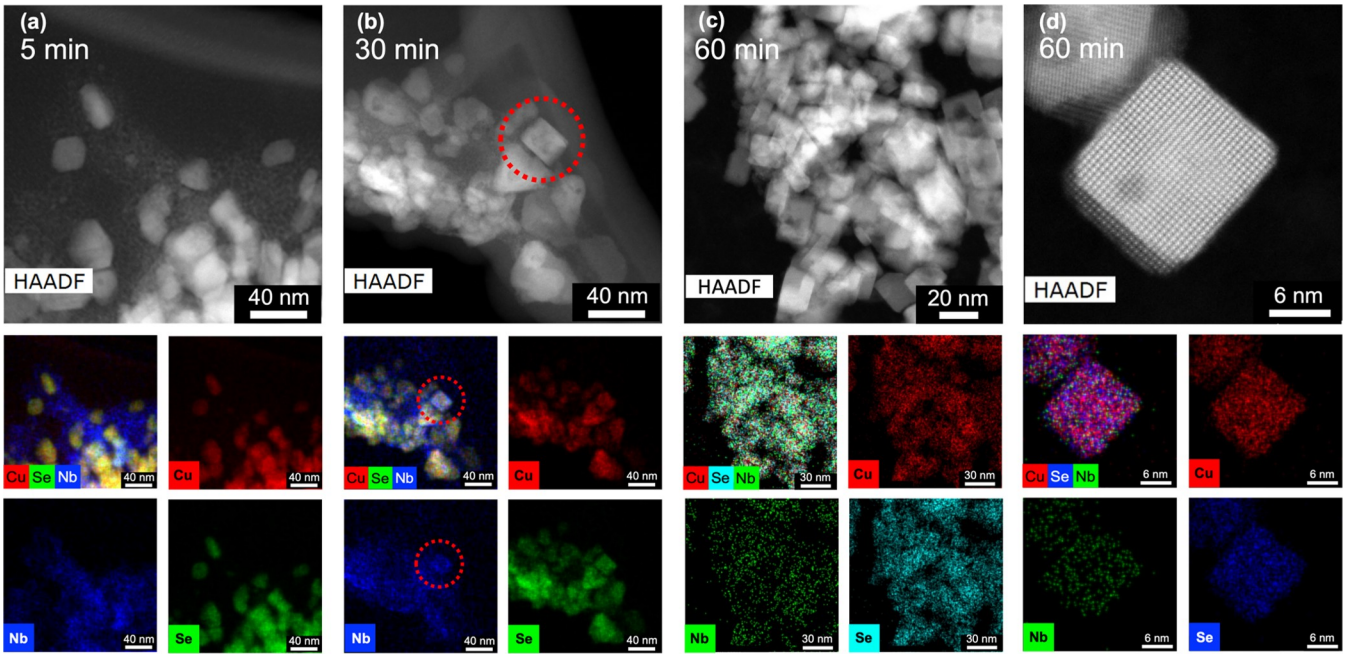

Figure 4. High-angle annular dark-field-STEM (HAADF-STEM) images and EDX mapping of the reaction products obtained upon Cu injection: (a) after 5 min, (b) after 30 min, (c) after 60 min low magnification, and (d) after 60 min high magnification.

seen from the EDX mapping, which is highlighted by the selected area (red dotted circle) in Figures 4b and S7 (SI). Nb is more concentrated at the surface and less concentrated at the core, suggesting a cation exchange process materialized by the Nb diffusion from the exterior of $Cu_{2-x}Se$, as evidenced in similar reports for cation exchange in $Cu_{2-x}Se$.[32] The formation of ternary Cu_3NbSe_4 nanoparticles within 30 min is also supported by the measured *d*-spacing of 0.58 Å measured in the TEM image (Figure S4), in agreement with the time-dependent XRD study. After 60 min, the reaction is completed as validated by a uniform element distribution, as shown in Figure 4c. The Nb matrix background shown at 5 and 30 min is no longer present. Furthermore, only cuboid Cu_3NbSe_4 nanoparticles could be observed after 60 min. A higher magnification image of a completely formed Cu_3NbSe_4 nanocuboid is shown in Figure 4d.

To monitor the progress of transformation, the reaction products obtained from 5, 30, and 60 min were investigated by Raman spectroscopy (Figure 5). The time-dependent Raman study is consistent with the time-dependent XRD and STEM-EDX studies results. In the first 5 min after the Cu injection, $Cu_{2-x}Se$ is the only identified product. After 30 min, the characteristic peaks of Cu_3NbSe_4 can be observed along with the peak of $Cu_{2-x}Se$. The reaction is completed after 60 min, illustrated by Raman spectroscopy, the spectrum showing only Cu_3NbSe_4 characteristic peaks. Synthesized $Cu_{2-x}Se$, prepared by the same method but without the Nb source, was used as a reference in this study. The Raman analysis of $Cu_{2-x}Se$ reveals a peak at 260 cm^{-1}, which matches to the characteristic peak reported in the literature.[33,34]

A proposed mechanism, derived from the nanocrystals formation studies, is illustrated in Figure 6. First, $NbSe_2$ is formed by reacting the Nb and Se precursors (Figure 6a) followed by the injection of a Cu precursor, which causes the $NbSe_2$ nanosheets to decompose, accompanied by the formation of the $Cu_{2-x}Se$ nanocrystals (Figure 6b). Given the concentration gradient observed in the STEM-EDX

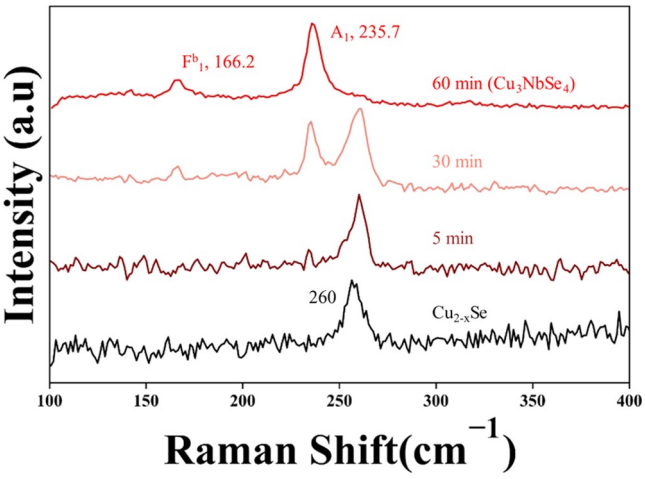

Figure 5. Raman spectra of reaction products obtained upon Cu injection: after 5, 30 min, and 60; pure $Cu_{2-x}Se$ (bottom spectrum) is used as a reference.

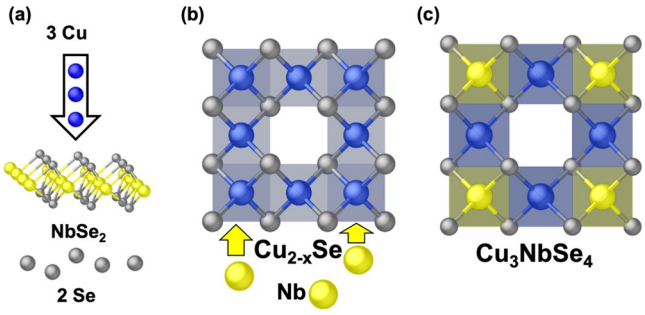

Figure 6. Scheme of the proposed Cu_3NbSe_4 formation mechanism: (a) $NbSe_2$ nanosheets are formed; the excess Se before the Cu injection is provided for stoichiometry reasons; Cu/Nb/Se 3:1:4. (b) $Cu_{2-x}Se$ forms and Nb is redissolved and (c) completed Cu_3NbSe_4 nanocrystal is formed.

https://doi.org/10.1021/acsnanoscienceau.2c00021
ACS Nanosci. Au 2022, 2, 440−447

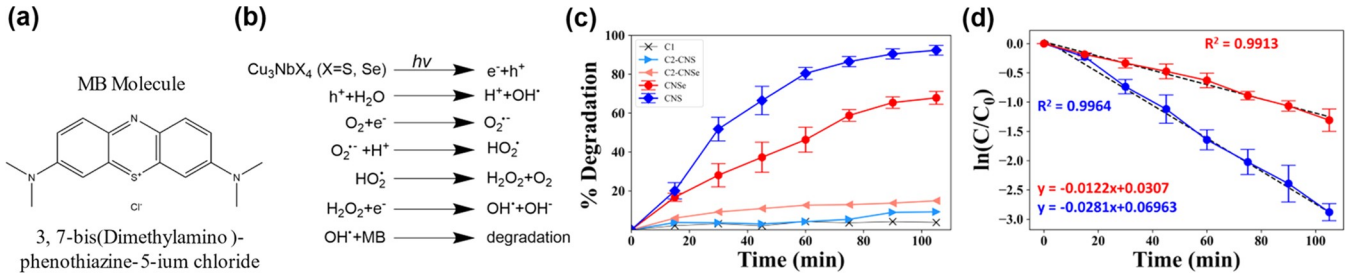

Figure 7. (a) Molecular structure and IUPAC name of MB. (b) Proposed steps of the photocatalysis mechanism for Cu_3NbX_4 (proposed based on refs 35 and 38). (c) MB % degradation plots calculated using absorbance at 664 nm with control groups C1 (without a photocatalyst) and C2 (without light); the main experiments were repeated three times and the error bars were generated using standard deviations. (d) Kinetics of the Cu_3NbX_4 photocatalytic reaction.

images, we posit that Nb diffuses into the $Cu_{2-x}Se$ lattice, partially replacing the Cu ion and leading to the new Cu_3NbSe_4 sulvanite crystal structure finally formed (Figure 6c).

Photocatalytic Activity

As a proof-of-concept of Nb sulvanites' potential as photocatalysts under visible light, methylene blue (MB, molecular structure shown in Figure 7a) was used to evaluate the photocatalytic activity of the synthesized Cu_3NbS_4 and Cu_3NbSe_4 under simulated sunlight. The MB photodegradation was monitored by UV−vis spectroscopy. In a typical experiment, the Cu_3NbS_4 or Cu_3NbSe_4 nanocrystal powder was dispersed in an MB solution, and the dispersion was placed in the dark for 30 min to reach adsorption/desorption equilibrium. Afterward, the suspension was exposed to the simulated sunlight under vigorous stirring, and aliquots were taken every 15 min. A possible mechanism of the photocatalytic reaction, adapted from literature, is outlined in Figure 7b.[35,38]

First, under illumination, the semiconductor photocatalyst generates electrons and holes, which then migrate to the surface of the nanoparticles. Upon reaching the surface, the charge carriers react with H_2O and the O_2 dissolved in the solution, leading to the formation of $OH^•$ radicals after consecutive electrochemical reactions. Finally, the $OH^•$ radicals react with the MB molecules and trigger the degradation of MB. The MB concentration decreased as the reaction with the $OH^•$ radicals progresses, leading to the decrease of the MB absorbance, as measured by UV−vis. The detailed MB photodegradation reaction mechanism had been studied extensively by different groups.[36−39] It is reported that the decomposition of MB involves aromatic ring openings and methyl group cleavage, resulting in various intermediates, ultimately leading to CO_2 as the final product. In this work, the MB disappearance provides the proof-of-concept that Cu_3NbS_4 and Cu_3NbSe_4 have potential in photocatalysis. Further studies on the degradation mechanism are in progress.

The recorded UV−vis absorbance at λ_{max} for MB, 664 nm,[40] was used for further analysis (Figure 7c). The % degradation is defined as follows

$$\%\ \text{degradation} = 1 - \frac{C_t}{C_0}$$

where C_t is the absorption of the sample at time t and C_0 is the absorption before the illumination. The analyses indicated that Cu_3NbS_4 (92.3 ± 2.5%) has better photocatalytic activity than Cu_3NbSe_4 (67.8 ± 3.3%) in MB photodegradation.

Two control experiments were conducted to better understand the contribution to the % degradation from the background (Figure 7c). First, a control experiment (C1, cross mark) was conducted by exposing the MB solution to the light source in the absence of the photocatalyst; no significant decomposition was observed (3.8%). Second, to decouple the contribution of light from the interaction between nanoparticles and the MB solution, control experiment 2 was conducted by dispersing the nanoparticles in the MB solution in the absence of light (C2, triangle mark).

The photodegradation rate can be described by the Langmuir−Hinshelwood kinetic model

$$v = -\frac{dC}{dt} = \frac{k_r K C_{eq}}{1 + K C_{eq}} \quad (1)$$

where k_r is the apparent reaction rate constant, K is the absorption coefficient of the substance to be degraded, and C_{eq} is the equilibrium concentration. For very low concentrations ($KC_{eq} \ll 1$), the equation can be simplified as the pseudo-first-order equation

$$\ln\left(\frac{C_t}{C_0}\right) = -kt \quad (2)$$

Using this equation, the MB photodegradation rate for the ligand exchanged Cu_3NbS_4 and Cu_3NbSe_4 were found to be 2.81×10^{-2} min^{-1} and 1.22×10^{-2} min^{-1} (Figure 7d). Given the smaller particle size of Cu_3NbSe_4 (Table S1) associated with a larger surface area, a higher catalytic rate was expected for Cu_3NbSe_4. A possible explanation for its lower catalytic activity could be ascribed to the passivation of the particle's surface during the ligand exchange, as a sulfide ligand is used for both compounds. The catalytic sites of Cu_3NbS_4 are fully accessible as the sulfide capping reagents do not impact the surface composition, whereas this is not the case for Cu_3NbSe_4. Further investigations to elucidate the difference in catalytic activity are ongoing.

To investigate the stability of the photocatalyst, the crystal structure of the Cu_3NbS_4 and Cu_3NbSe_4 before and after the photocatalytic test was evaluated by XRD. No obvious structural or crystallinity changes are observed after the photocatalytic test (Figure 1a,b), and no impurity peaks were observed, suggesting that the catalyst could be recycled.

CONCLUSIONS

A solution-based method to synthesize Cu_3NbX_4 (X = S, Se) nanocrystals at a low temperature (300 °C) is presented in this work. XRD and Raman measurements were used to character-

https://doi.org/10.1021/acsnanoscienceau.2c00021
ACS Nanosci. Au 2022, 2, 440−447

ize the nanomaterials and assess their purity. The formation mechanism of the Cu_3NbSe_4 nanocrystals synthesized using $NbSe_2$ nanosheets as a starting material was investigated by XRD and STEM-EDX. TEM showed that the synthesized Cu_3NbS_4 and Cu_3NbSe_4 nanocrystals exhibit cuboid morphology. UV−vis spectra of Cu_3NbS_4 and Cu_3NbSe_4 were compared to the DFT-simulated spectra, which confirmed the presence of the three absorption peaks. Photocatalytic activity of the synthesized Cu_3NbS_4 and Cu_3NbSe_4 nanoparticles was studied using methylene blue degradation as a proof-of-concept for niobium sulvanite nanoparticles' potential as photocatalysts.

EXPERIMENTAL METHODS

Reagents

Carbon disulfide (CS_2, 99.9%, Sigma-Aldrich), chloroform ($CHCl_3$, 99.9%, Fisher), copper(II) chloride dihydrate ($CuCl_2{\cdot}2H_2O$, 99%, Sigma-Aldrich), methylene blue (RICCA, surfactant analysis), 1-dodecanethiol (1-DDT, 98%, Aldrich), ethanol (EtOH, anhydrous, Decon), niobium(V) chloride ($NbCl_5$, 99%, Aldrich), selenium powder (Se, 99.99%, Aldrich), 1-octadecene (ODE, 90%, Aldrich), oleylamine (OLA, 70%, Aldrich), and ammonium sulfide (aqueous $(NH4)_2S$ solution, 20−24%, Alfa Aesar) were all used as received, without further purification.

Note. Standard Schlenk line techniques were used for all syntheses. Inhalation of CS_2 can cause serious health problems, and therefore it is recommended to perform all synthetic steps in a fume hood, wearing appropriate personal protective equipment.

Synthesis of NbS_2 Nanosheets

The Nb precursor was prepared by loading $NbCl_5$ (0.5 mmol) and OLA (15 mL) into a 100 mL round-bottom flask, which was further degassed at 120 °C for 30 min under a vacuum and then filled with argon gas. The S precursor was prepared by mixing 1-DDT (1 mL) and OLA (4 mL) in a 25 mL round-bottom flask, degassing at room temperature for 30 min, and then filling with argon gas. After the Nb precursor reached 300 °C, the degassed sulfur precursor was mixed with 0.5 mL of CS_2 before the injection, and this mixture was slowly injected into the Nb precursor solution. After the injection, the reaction was stirred at 300 °C for 1 h and then allowed to cool to room temperature by removing the heating source. The resulting nanosheets were washed three times using $CHCl_3$/EtOH at a 1:3 volume ratio. The final product was dried in a vacuum oven and stored in ambient conditions.

Synthesis of Cu_3NbS_4 Nanocrystals

The synthesis procedure for Cu_3NbS_4 largely follows the steps described for the NbS_2 nanosheets, but with a few additional steps before cooling. After the Nb and S precursors reacted at 300 °C for 1 h, a separately prepared Cu precursor containing $CuCl_2{\cdot}2H_2O$ (1.5 mmol) dissolved in OLA (6 mL) was injected into the reaction flask. After 10 min, 0.5 mL of CS_2 was added to the flask. The mixture was stirred at 300 °C for 2 more hours and then allowed to cool to room temperature by removing the heating source. The resulting Cu_3NbS_4 nanocrystals were washed three times using $CHCl_3$/EtOH at a 1:3 volume ratio. The final product was dried in a vacuum oven for further characterization.

Synthesis of $NbSe_2$ Nanosheets

First, the Se precursor was prepared by dissolving selenium powder (1 mmol) in a mixture of ODE (5 mL) and OLA (10 mL) in a 100 mL flask. The solution was further degassed at 120 °C for 30 min under a vacuum. Afterward, this Se precursor solution was heated to 300 °C under an argon atmosphere. Meanwhile, the Nb precursor was prepared by degassing the mixture of $NbCl_5$ (0.5 mmol) and OLA (6 mL) at 120 °C for 30 min under vacuum and then filled with argon. Next, the Nb precursor was injected into the Se precursor at 300 °C under argon. The mixture was stirred at 300 °C for 1 h and then allowed to naturally cool to room temperature by removing the heating source. The resulting nanosheets were washed three times using $CHCl_3$/EtOH at a 1:3 volume ratio. The final product was dried in a vacuum oven and stored in ambient conditions.

Synthesis of Cu_3NbSe_4 Nanocrystals

The procedure for Cu_3NbSe_4 largely follows the steps involved in the $NbSe_2$ nanosheets but the amount of Se was increased to 2 mmol to meet the final stoichiometry ratio of Cu/Nb/Se = 3:1:4. After the Se and Nb precursors have been mixed and reacted at 300 °C for 1 h, a separately prepared Cu precursor containing $CuCl_2{\cdot}2H_2O$ (1.5 mmol) and OLA (6 mL) was injected at 300 °C. After the injection, the reaction was stirred at 300°C for 1 h and then allowed to cool to room temperature by removing the heating source. The resulting Cu_3NbSe_4 nanocrystals were washed three times using $CHCl_3$/EtOH at a 1:3 volume ratio. The final product was dried in a vacuum oven and stored in ambient conditions.

Characterization

High-resolution transmission electron microscopy (HRTEM) images were recorded using a Phillips CM200 instrument. STEM-EDX and HDAAF images were obtained on a Thermo Fisher Talos F200X and a Titan G2 scanning/transmission electron microscope. X-ray diffraction (XRD) was performed on a Rigaku MiniFlex with a Cu Kα radiation source (λ = 1.5405 Å) and operated at 40 mV and 30 mA. Raman measurements were conducted on a WITec α 300 Raman microscope equipped with a 532 nm laser. UV−vis−NIR were collected using a Shimadzu UV-3600 Plus spectrophotometer.

Ligand Exchange

The as-synthesized Cu_3NbX_4 nanoparticles have hydrophobic ligands originating from the synthesis attached to the surface. Therefore, a ligand exchange step that confers nanoparticles to a hydrophilic surface is necessary to enable uniform dispersion of the Cu_3NbX_4 in the MB aqueous solution. The ligand exchange process follows a method adapted from the literature.[41] Exemplified here for the Cu_3NbSe_4, the same process was conducted for the Cu_3NbS_4. First, the dried Cu_3NbSe_4 powder (180 mg) was dispersed in toluene (40 mL) using a probe ultrasonicator. Next, 5 mL of an ammonium sulfide $(NH_4)_2S$ aqueous solution was added to the dispersion leading to a clear phase separation: on the top, Cu_3NbX_4 was dispersed in toluene, and at the bottom, the clear ammonium sulfide solution. The mixed dispersion was shaken for 1 min and allowed to settle until another phase separation occurred: clear toluene on top and Cu_3NbSe_4 dispersed in ammonium sulfide at the bottom. This indicated that the hydrophobic ligands attached to the particle surface were replaced by S^{2+}. The aqueous phase containing the Cu_3NbX_4 nanoparticles was separated and subjected to centrifugation. The particles were collected and dried in a vacuum oven for further use. After this ligand exchange, the nanoparticles could be dispersed in polar solvents.

Photocatalytic Test

The ligand exchanged Cu_3NbX_4 powder (20 mg) was mixed with 30 mL of an MB stock solution (0.66 mg/mL) and the solution was placed in the dark under continuously stirring for 30 min to reach the adsorption−desorption equilibrium. Then, the solution was exposed to the simulated sunlight (Oriel, LCS-100 AM1.5G operation at 1.0 sun output) for 105 min, while 1 mL aliquots were collected every 15 min. The UV−vis spectra of the collected aliquots were recorded to determine the remaining MB amount. Compared to other well-documented photocatalytic materials such as anatase- and rutile-TiO_2, the sulvanites have smaller band gaps, which can generate electron and hole pairs via visible-light wavelength irradiation, making them promising sunlight photocatalysts. As a proof-of-concept, a solar simulator was used for studying MB degradation. Both Cu_3NbS_4 and Cu_3NbSe_4 degraded the MB efficiently.

https://doi.org/10.1021/acsnanoscienceau.2c00021
ACS Nanosci. Au 2022, 2, 440−447

■ ASSOCIATED CONTENT

Supporting Information

The Supporting Information is available free of charge at https://pubs.acs.org/doi/10.1021/acsnanoscienceau.2c00021.

Brief description of the computational methods, particle size distribution, HRTEM of the time-dependent mechanism study at 5 and 30 min, synthesized $NbSe_2$ characterization, discussion of size and strain impact on the XRD diffraction pattern of Cu_3NbSe_4, and EDX data for Cu_3NbSe_4 (PDF)

■ AUTHOR INFORMATION

Corresponding Authors

Cheng-Yu Lai − *Department of Mechanical and Materials Engineering, Florida International University, Miami, Florida 33174, United States;* orcid.org/0000-0002-8931-5601; Email: clai@fiu.edu

Daniela R. Radu − *Department of Mechanical and Materials Engineering, Florida International University, Miami, Florida 33174, United States;* orcid.org/0000-0001-6833-5825; Email: dradu@fiu.edu

Authors

Chen-Yu Chang − *Department of Mechanical and Materials Engineering, Florida International University, Miami, Florida 33174, United States*

Roberto Prado-Rivera − *Department of Mechanical and Materials Engineering, Florida International University, Miami, Florida 33174, United States;* orcid.org/0000-0002-3376-6673

Mimi Liu − *Department of Mechanical and Materials Engineering, Florida International University, Miami, Florida 33174, United States*

Complete contact information is available at: https://pubs.acs.org/10.1021/acsnanoscienceau.2c00021

Author Contributions

This manuscript was written through the contributions of all authors. All authors have given approval to the final version of the manuscript.

Funding

The material is based upon work supported by: NASA under NASA Cooperative Agreement Award No. 80NSSC19M0201, NASA Cooperative Agreement Award No. 80NSSC21M0310, NASA Graduate Fellowship Award for Roberto Prado-Rivera, Award No. 80NSSC20K1462, and the National Science Foundation, Awards NSF CBET-1924412 and DMR-2122078.

Notes

The authors declare no competing financial interest.

■ ACKNOWLEDGMENTS

The authors acknowledge Dr. Ke Wang and Dr. Danielle Hickey at Pennsylvania State University for the STEM-EDX work.

■ REFERENCES

(1) Kehoe, A. B.; Scanlon, D. O.; Watson, G. W. Modelling potential photovoltaic absorbers Cu3MCh4(M = V, Nb, Ta; Ch = S, Se, Te) using density functional theory. *J. Phys.: Condens. Matter* **2016**, *28*, No. 175801.

(2) Kehoe, A. B.; Scanlon, D. O.; Watson, G. W. The electronic structure of sulvanite structured semiconductors Cu3MCh4(M = V, Nb, Ta; Ch = S, Se, Te): prospects for optoelectronic applications. *J. Mater. Chem. C* **2015**, *3*, 12236−12244.

(3) Chen, E. M.; Stoyko, S. S.; Aitken, J. A.; Poudeu, P. F. P. Tuning the optical, electronic and thermal properties of Cu3NbS4-xSex through chemical substitution. *Inorg. Chem. Front.* **2017**, *4*, 1493−1500.

(4) Pauling, L.; Hultgren, R. The Crystal Structure of Sulvanite, Cu_3VS_4. *Z. Kristallogr. - Cryst. Mater.* **1933**, *84*, 204−212.

(5) Arribart, H.; Sapoval, B.; Gorochov, O.; LeNagard, N. Fast ion transport at room temperature in the mixed conductor Cu3VS4. *Solid State Commun.* **1978**, *26*, 435−439.

(6) Polizzotti, A.; Repins, I. L.; Noufi, R.; Wei, S.-H.; Mitzi, D. B. The state and future prospects of kesterite photovoltaics. *Energy Environ. Sci.* **2013**, *6*, 3171−3182.

(7) Barkhouse, D. A. R.; Gunawan, O.; Gokmen, T.; Todorov, T. K.; Mitzi, D. B. Device characteristics of a 10.1% hydrazine-processed Cu2ZnSn(Se,S)4 solar cell. *Prog. Photovoltaics* **2012**, *20*, 6−11.

(8) Altamura, G.; Wang, M.; Choy, K.-L. Influence of alkali metals (Na, Li, Rb) on the performance of electrostatic spray-assisted vapor deposited Cu2ZnSn(S,Se)4 solar cells. *Sci. Rep.* **2016**, *6*, No. 22109.

(9) Altermatt, P. P.; Kiesewetter, T.; Ellmer, K.; Tributsch, H. Specifying targets of future research in photovoltaic devices containing pyrite (FeS2) by numerical modelling. *Sol. Energy Mater. Sol. Cells* **2002**, *71*, 181.

(10) Chen, C.-C.; Stone, K. H.; Lai, C.-Y.; Dobson, K. D.; Radu, D. Sulvanite (Cu3VS4) nanocrystals for printable thin film photovoltaics. *Mater. Lett.* **2018**, *211*, 179−182.

(11) Liu, M.; Lai, C.-Y.; Chang, C.-Y.; Radu, D. R. Solution-Based Synthesis of Sulvanite Cu3TaS4 and Cu3TaSe4 Nanocrystals. *Crystals* **2021**, *11*, 51.

(12) Liu, M.; Lai, C.-Y.; Zhang, M.; Radu, D. R. Cascade synthesis and optoelectronic applications of intermediate bandgap Cu3VSe4 nanosheets. *Sci. Rep.* **2020**, *10*, No. 21679.

(13) Liu, M.; Lai, C.-Y.; Selopal, G. S.; Radu, D. R. Synthesis and optoelectronic properties of Cu3VSe4 nanocrystals. *PLoS One* **2020**, *15*, No. e0232184.

(14) Lv, X. S.; Deng, Z. H.; Miao, F. X.; Gu, G. X.; Sun, Y. L.; Zhang, Q. L.; Wan, S. M. Fundamental optical and electrical properties of nano-Cu3VS4 thin film. *Opt. Mater.* **2012**, *34*, 1451−1454.

(15) Liu, Y.; Ding, T.; Luo, X.; Li, Y. L.; Long, J. L.; Wu, K. F. Tuning Intermediate-Band Cu3VS4 Nanocrystals from Plasmonic-like to Excitonic via Shell-Coating. *Chem. Mater.* **2020**, *32*, 224−233.

(16) Mantella, V.; Ninova, S.; Saris, S.; Loiudice, A.; Aschauer, U.; Buonsanti, R. Synthesis and Size-Dependent Optical Properties of Intermediate Band Gap Cu3VS4 Nanocrystals. *Chem. Mater.* **2019**, *31*, 532−540.

(17) Prado-Rivera, R.; Chang, C.-Y.; Liu, M.; Lai, C.-Y.; Radu, D. R. Sulvanites: The Promise at the Nanoscale. *Nanomaterials* **2021**, *11*, 823.

(18) Kars, M.; Rebbah, A.; Rebbah, H. Cu3NbS4. *Acta Crystallogr., Sect. E: Struct. Rep. Online* **2005**, *61*, I180−I181.

(19) Grima-Gallardo, P.; Salas, M.; Contreras, O.; Power, C.; Quintero, M.; Cabrera, H.; Zumeta-Dube, I.; Rodriguez, A.; Aitken, J.; Bramer-Escamilla, W. Cu3TaSe4 and Cu3NbSe4: X-ray diffraction, differential thermal analysis, optical absorption and Raman scattering. *J. Alloys Compd.* **2016**, *658*, 749−756.

(20) Ikeda, S.; Aono, N.; Iwase, A.; Kobayashi, H.; Kudo, A. Cu3 MS4 (M=V, Nb, Ta) and its Solid Solutions with Sulvanite Structure for Photocatalytic and Photoelectrochemical H2 Evolution under Visible-Light Irradiation. *ChemSusChem* **2019**, *12*, 1977−1983.

(21) Hersh, P. A. *Wide Band Gap Semiconductors and Insulators: Synthesis, Processing and Characterization*, Ph.D.; Oregon State University: Ann Arbor, 2007.

(22) Li, Y.; Wu, M.; Zhang, T.; Qi, X.; Ming, G.; Wang, G.; Quan, X.; Yang, D. Natural sulvanite Cu3MX4 (M = Nb, Ta; X = S, Se):

Promising visible-light photocatalysts for water splitting. *Comput. Mater. Sci.* **2019**, *165*, 137−143.
(23) Shaikh, J. S.; Shaikh, N. S.; Mishra, Y. K.; Kanjanaboos, P.; Shewale, P. M.; Sabale, S.; Praserthdam, S.; Lokhande, C. D. Low-cost Cu-based inorganic hole transporting materials in perovskite solar cells: Recent progress and state-of-art developments. *Mater. Today Chem.* **2021**, *20*, No. 100427.
(24) Uheida, A.; Mohamed, A.; Belaqziz, M.; Nasser, W. S. Photocatalytic degradation of Ibuprofen, Naproxen, and Cetirizine using PAN-MWCNT nanofibers crosslinked TiO2-NH2 nanoparticles under visible light irradiation. *Sep. Purif. Technol.* **2019**, *212*, 110−118.
(25) Thakur, S.; Das, P.; Mandal, S. K. Solvent-Induced Diversification of CdS Nanostructures for Photocatalytic Degradation of Methylene Blue. *ACS Appl. Nano Mater.* **2020**, *3*, 5645−5655.
(26) El-Katori, E. E.; Ahmed, M. A.; El-Bindary, A. A.; Oraby, A. M. Impact of CdS/SnO2 heterostructured nanoparticle as visible light active photocatalyst for the removal methylene blue dye. *J. Photochem. Photobiol., A* **2020**, *392*, No. 112403.
(27) Espinosa-García, W.; Valencia-Balvín, C.; Osorio-Guillén, J. M. Phononic and thermodynamic properties of the sulvanite compounds: A first-principles study. *Comput. Mater. Sci.* **2016**, *113*, 275−279.
(28) Nath, D.; Singh, F.; Das, R. X-ray diffraction analysis by Williamson-Hall, Halder-Wagner and size-strain plot methods of CdSe nanoparticles- a comparative study. *Mater. Chem. Phys.* **2020**, *239*, No. 122021.
(29) Mote, V. D.; Purushothani, Y.; Dole, B. N. Williamson-Hall analysis in estimation of lattice strain in nanometer-sized ZnO particles. *J. Theor. Appl. Phys.* **2012**, *6*, No. 6.
(30) Bindu, P.; Thomas, S. Estimation of lattice strain in ZnO nanoparticles: X-ray peak profile analysis. *J. Theor. Appl. Phys.* **2014**, *8*, 123−134.
(31) Nasiri-Tabrizi, B. Thermal treatment effect on structural features of mechano-synthesized fluorapatite-titania nanocomposite: A comparative study. *J. Adv. Ceram.* **2014**, *3*, 31−42.
(32) Gariano, G.; Lesnyak, V.; Brescia, R.; Bertoni, G.; Dang, Z.; Gaspari, R.; De Trizio, L.; Manna, L. Role of the Crystal Structure in Cation Exchange Reactions Involving Colloidal Cu2Se Nanocrystals. *J. Am. Chem. Soc.* **2017**, *139*, 9583−9590.
(33) Cho, A.; Ahn, S.; Yun, J. H.; Gwak, J.; Ahn, S. K.; Shin, K.; Yoo, J.; Song, H.; Yoon, K. The growth of $Cu_{2-x}Se$ thin films using nanoparticles. *Thin Solid Films* **2013**, *546*, 299−307.
(34) Lesnyak, V.; Brescia, R.; Messina, G. C.; Manna, L. Cu Vacancies Boost Cation Exchange Reactions in Copper Selenide Nanocrystals. *J. Am. Chem. Soc.* **2015**, *137*, 9315−9323.
(35) Harris, J.; Silk, R.; Smith, M.; Dong, Y.; Chen, W.-T.; Waterhouse, G. I. N. Hierarchical TiO2 Nanoflower Photocatalysts with Remarkable Activity for Aqueous Methylene Blue Photo-Oxidation. *ACS Omega* **2020**, *5*, 18919−18934.
(36) Nguyen, C. H.; Fu, C.-C.; Juang, R.-S. Degradation of methylene blue and methyl orange by palladium-doped TiO2 photocatalysis for water reuse: Efficiency and degradation pathways. *J. Cleaner Prod.* **2018**, *202*, 413−427.
(37) Rauf, M. A.; Meetani, M. A.; Khaleel, A.; Ahmed, A. Photocatalytic degradation of Methylene Blue using a mixed catalyst and product analysis by LC/MS. *Chem. Eng. J.* **2010**, *157*, 373−378.
(38) Houas, A. Photocatalytic degradation pathway of methylene blue in water. *Appl. Catal., B* **2001**, *31*, 145−157.
(39) Zuo, R.; Du, G.; Zhang, W.; Liu, L.; Liu, Y.; Mei, L.; Li, Z. Photocatalytic Degradation of Methylene Blue Using TiO2Impregnated Diatomite. *Adv. Mater. Sci. Eng.* **2014**, *2014*, 1−7.
(40) Ayad, M. M.; El-Nasr, A. A. Adsorption of Cationic Dye (Methylene Blue) from Water Using Polyaniline Nanotubes Base. *J. Phys. Chem. C* **2010**, *114*, 14377−14383.
(41) Nag, A.; Kovalenko, M. V.; Lee, J.-S.; Liu, W.; Spokoyny, B.; Talapin, D. V. Metal-free Inorganic Ligands for Colloidal Nanocrystals: S2−, HS−, Se2−, HSe−, Te2−, HTe−, TeS32−, OH−, and NH2− as Surface Ligands. *J. Am. Chem. Soc.* **2011**, *133*, 10612−10620.

https://doi.org/10.1021/acsnanoscienceau.2c00021
ACS Nanosci. Au 2022, 2, 440−447